The published manuscript is available at EurekaSelect via doi.org/10.2174/0929867328666210910141316

The anti-proliferative potential of fluorinated curcumin analogues: experimental and computational analysis and review of the literature

Mahdi Hatamipour[1,2], Farzin Hadizadeh[2,3*], Mahmoud Reza Jaafari[1,3], Zahra Khashyarmanesh[3], Thozhukat Sathyapalan[4], Amirhossein Sahebkar[2,5,6*]

[1]Nanotechnology Research Center, Pharmaceutical Technology Institute, Mashhad University of Medical Sciences, Mashhad, Iran

[2]Biotechnology Research Center, Pharmaceutical Technology Institute, Mashhad University of Medical Sciences, Mashhad, Iran

[3]Department of Medicinal Chemistry, School of Pharmacy, Mashhad University of Medical Sciences, Mashhad, Iran

[3]Academic Diabetes, Endocrinology and Metabolism, Hull York Medical School, University of Hull, UK.

[4]Biotechnology Research Center, Pharmaceutical Technology Institute, Mashhad University of Medical Sciences, Mashhad, Iran

[5]Applied Biomedical Research Center, Mashhad University of Medical Sciences, Mashhad, Iran

[6]School of Pharmacy, Mashhad University of Medical Sciences, Mashhad, Iran

Correspondence: hadizadehf@mums.ac.ir; sahebkara@mums.ac.ir

Funding source: This project was financially supported by the Mashhad University of Medical Sciences Research Council (Mashhad, Iran). This project has been conducted by a grant from Cancer research center of cancer institute of Iran (Shams cancer charity, Grant No: 37312-202-01-97) and a Grant No. 960206 of the Biotechnology Development Council of the Islamic Republic of Iran.

Conflict of Interests: None.

Abstract

Background: Curcuminoids, flavoring and coloring agents in food have potent antioxidant, anti-tumor activity and anti-inflammatory effects. However, they are rapidly metabolized to lesser active metabolites. Therefore, various studies have been conducted to synthesize new and stable curcumin analogues with enhanced therapeutic activity.

Methods: Fluorinated curcumin compounds (**2a**-**2f**) were synthesized by Knoevenagel condensation between fluorobenzaldehydes (**1a**-**1f**) with curcumin. Fluorinated demethoxycurcumin (**3a**) was synthesized by condensation between demethoxycurcumin and 3,4-difluorobenzaldehyde (**1f**). The structures of these compounds were confirmed by FT-IR, ^{1}H-NMR, ^{13}C-NMR, ^{19}FNMR and mass spectroscopy. Antiproliferative activities of these synthetic compounds were evaluated against breast cancer cells (4T1), melanoma cancer cells (B16F10) and normal cell lines (NIH 3T3) using MTT assay. The interaction of curcumin, **2f** and **3a** with several proteins (1HCL, 2ZOQ, 3D94, 5EW3, 4WA9, 1XKK, 6CCY) was investigated. The structural preservation of the epidermal growth factor receptor (EGFR) was investigated by molecular dynamics simulation.

Results: The spectroscopic data obtained confirmed the proposed structure of fluorinated analogues. The results showed that compounds **2f** and **3a** inhibited cancer cells proliferation significantly more than other compounds. Compounds **2f** and **3a** showed the highest affinity and lowest binding energy with EGFR. The binding energies were -7.8, -10 and -9.8 kcal/mol for curcumin, **2f** and **3a** with EGFR, respectively. The molecular docking results demonstrated that compounds **2f** and **3a** were firmly bound in a complex with EGFR via the formation of a hydrogen bond.

Conclusion: In summary, we found that fluorinated demethoxycurcumin and fluorinated curcumin induced cancer cells death and bind to EGFR with high affinity.

Keywords: Curcumin; Demethoxycurcumin; Tumor; Breast cancer

1 Introduction

Curcuminoids are phenolic compounds commonly used in India and China as traditional medicines and additives in food. The main curcuminoids are curcumin, desmethoxycurcumin (DMC) and bisdemethoxycurcumin (BDMC). In the last decade, curcuminoids were widely studied for their anticancer properties (1). The poor bioavailability and low aqueous solubility of curcumin limited its therapeutic activity (2). Anand et al. reported that the active methylene group enhances the degradation of curcumin in biological fluids (2). Tomren et al. suggested that destruction, low absorption, and fast metabolism of curcumin could be attributed to the presence of the methylene group and b-diketone moiety(3, 4). Numerous studies were carried out to synthesize new structurally modified curcumin derivatives with improved bioavailability and therapeutic activity. Recently, many studies reported novel curcumin derivatives with enhanced properties by substituting the 1,6-heptadiene group (5, 6) and central methylene proton with the benzylidene group. It has been shown that 4-arylidene analogues inhibited cancer cells more than curcumin by inhibiting IKK/NF-κB (7). One study reported that the metabolic stability of the C – F bond is much higher than the C-H or C – OH bond. Consequently, fluorinated curcumins were synthesized via substitution of 4-arylidene groups (8). Recent studies revealed that fluorinated curcumin with improved stability inhibited cell growth in both colon and pancreatic cells. It also found that difluorinated curcumin (CDF) induced apoptosis in pancreatic BxPC-3 cells better than curcumin (9). Demethoxycurcumin (DMC), one of the main curcuminoids, differs from curcumin in the number of methoxy groups on the aromatic ring. Kunnumakkara et al. reported that this small change improved the stability of the chemical structure of DMC relative to curcumin (10). Besides, Katsidoni et al. demonstrated that DMC is more stable and efficient than curcumin (11). Recently, it has been shown that DMC strongly inhibited cancer cells by modulating P-gp, inhibiting cell proliferation, inducing apoptosis, inhibiting adhesion, reducing ECM, inducing degradation of MMP-9, MT1-MMP, uPA, inhibiting invasion and transcription of DNA. Yodkeeree et al. (12) investigated the anti-cancer activity of three curcuminoids and showed that DMC prevents cancer cell invasion more than curcumin. In addition, it was found that DMC exhibited more robust WIF-1 hypomethylation activity and was a more potent AMPK activator than curcumin (13, 14). In comparison with curcumin, Weiting et al. showed that DMC combined with photodynamic therapy (PDT) induced cancer cell death and showed more antiproliferative activity by triggering AMPK generation and ROS production (15). Computational approaches, including molecular docking and

molecular dynamic simulation, are instrumental in assessing ligand-protein interaction. These approaches are becoming popular because it is expensive to evaluate complex structures experimentally. Analytical methods have improved in efficiency and strength over the years, and these methods now play an essential role in the design of structure-based medicinal products. In this study, we present the synthesis of new curcumin and demethoxycurcumin analogous, assessing the antiproliferative activity of synthesized compounds and evaluating ligand-protein by computational approaches.

2 Materials and method

The reagents, chemicals, and solvents were obtained from Merck and Sigma-Aldrich. Curcumin and Demethoxycucumin were obtained from Sami Labs (Bangalore, India). RPMI 1640 medium and Fetal bovine serum were obtained from Gibco-BRL (St. Louis, MO). The tetrazolium dye MTT was purchased from Sigma-Aldrich (St Louis, USA). The determination content of synthesized compounds and reaction monitoring were performed with an HPLC system (Shimadzu, Kyoto, Japan) at 365 nm equipped with a TMS-C18 column (5 m, 4.6 mm 150 mm). in isocratic mode, the analysis was carried out by using THF (v/v, 50%) and citric acid 1mg/ml (v/v, 50%) at a flow rate of 1ml/min. Nuclear magnetic resonance (NMR) data were run in d6-DMSO and recorded on a Bruker 400 (^{1}H, 300 MHz; ^{13}C, 75 MHz) spectrometer. The mass analysis was performed using a Q-trap 3200 analyzer (AB SCIEX, Seattle, USA). The FTIR spectra were run on a Perkin Elmer (Waltham, Massachusetts, USA) spectroscopy.

2.1 The general method for synthesis and characterization of curcumin derivatives (*2a-2f and 3a*)

The Knoevenagel condensation, described in detail elsewhere (7), was used to prepare curcumin derivatives (Figure 1). Briefly, to a solution of curcumin (368 mg, 1mmol) or desmethoxycurcumin (DMC) (338 mg, 1mmol) and piperidine (50µl, 0.05mmol) in MeOH was added fluorinated benzaldehyde (**1a-1f** for curcumin and **1f** for DMC, 1mmol). The reaction mixture was stirred at room temperature under a nitrogen stream for 48 h. Upon completion reaction (monitored by HPLC), the solvent was removed by rotary evaporator and the unreacted regent was washed with $CHCl_3$: hexane (9:1) and dried to yield fluorinated derivatives (**2a-2f** and **3a**).

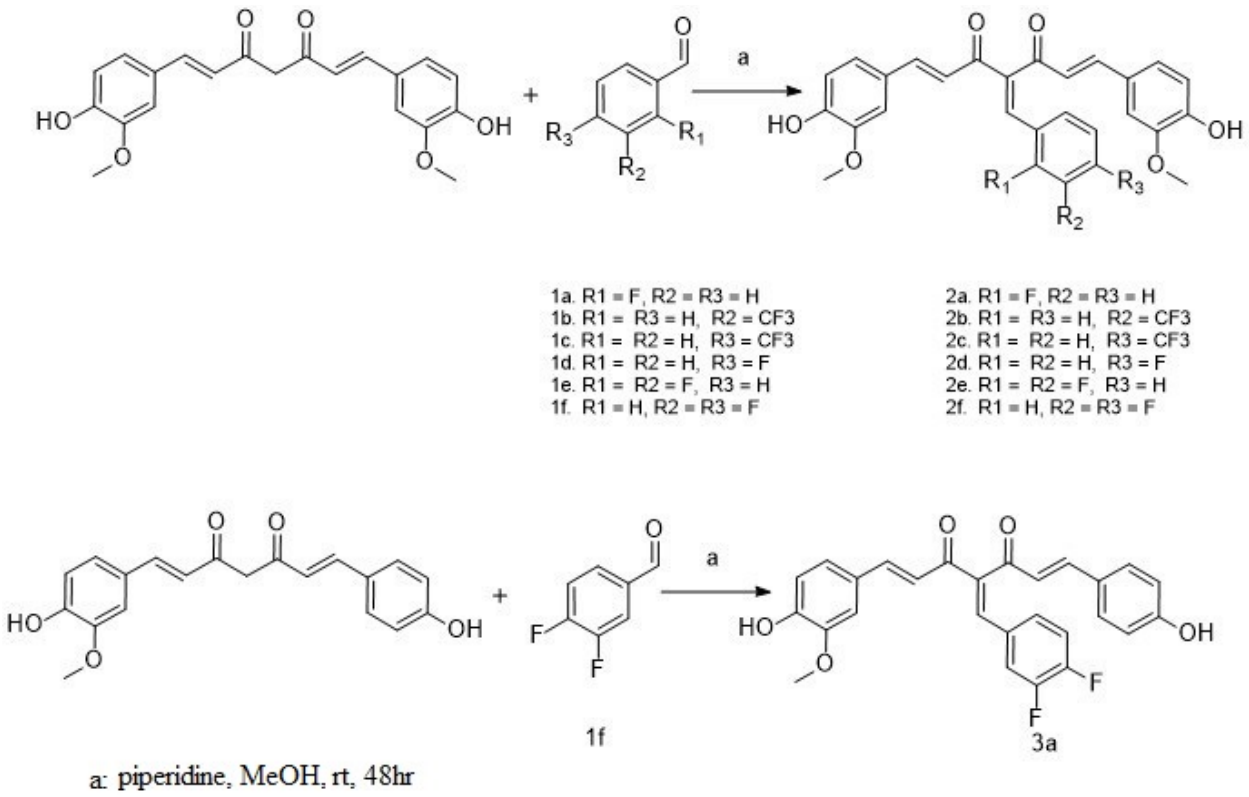

Figure 1

2.1.1 (1E,6E)-4-(2-fluorobenzylidene)-1,7-bis(4-hydroxy-3-methoxyphenyl) hepta-1,6-diene-3,5-dione (2a)

Yellow solid; Chemical Formula: $C_{28}H_{23}FO_6$; yield: 35%; mp: 170-172 ºC; IR (KBr, cm^{-1}): υ 3308, 2962, 1632, 1570, 1516, 1458, 1268. ^{1}H NMR (300 MHz, DMSO-d_6) δ 9.80 (s, 2H, OH), 8.05 (s, 1H), 7.68 (m, 1H), 7.49-7.28 (m, 8H, Ar-H), 7.23 (m, 1H), 7.11 (d, J = 8.2 Hz, 1H), 6.95 – 6.83 (m, 2H), 6.80 (d, J = 8.2 Hz, 1H), 3.87 (s, 3H, OCH_3), 3.81 (s, 3H, OCH_3). ^{13}C NMR (75 MHz, DMSO-d6) δ 196.65, 188.39, 160.49 (d, J = 250.3 Hz), 150.61, 150.49, 148.48, 147.50, 145.80, 143.86, 132.73, 132.10, 130.45, 126.46, 125.92, 125.26, 124.67, 124.52, 124.45, 122.33, 119.03, 116.54, 116.26, 116.20, 116.09, 112.60, 112.00, 56.29, 56.16. ^{19}F NMR (280 MHz, DMSO-d6) δ -112.50 (m, 1F). ESI-MS $[M+H]^+$ m/z: 475.

2.1.2 (1E,6E)-1,7-bis(4-hydroxy-3-methoxyphenyl)-4-(3-(trifluoromethyl)benzylidene)hepta-1,6-diene-3,5-dione (2b)

Yellow solid; Chemical Formula: $C_{29}H_{23}F_3O_6$; yield: 80%; mp: 184-186 ºC. IR (KBr, cm^{-1}): υ 3298, 2962, 1633, 1570, 1511, 1428, 1273, 1170, 1117. ^{1}H NMR (300 MHz, DMSO) δ 9.81 (s, 2H, OH), 8.14 (s, 1H), 7.81 (d, *J* = 8.4 Hz, 2H, Ar-H), 7.75 (d, *J* = 8.4 Hz, 2H, Ar-H), 7.72 – 7.53 (m, 2H, Ar-H), 7.50 – 7.39 (m, 2H, Ar-H), 7.33 (d, *J* = 8.2 Hz, 2H, Ar-H), 7.12 (d, *J* = 8.2 Hz, 1H, Ar-H), 6.97 – 6.85 (m, 2H), 6.80 (m, 1H), 3.88 (s, 3H, OCH_3), 3.81 (s, 3H, OCH_3). ^{13}C NMR (75 MHz, DMSO) δ 197.22, 188.51, 150.68, 150.47, 148.48, 148.45, 147.99, 145.59, 143.84, 138.38, 138.06, 130.81, 130.11(q, *J* = 31.5 Hz), 126.55, 126.30 , 126.15, 126.10, 125.90, 124.72, 124.55, 124.38(q, J = 270 Hz), 124.34, 118.68, 116.23, 116.10, 112.77, 112.14, 56.32, 56.14. ^{19}F NMR (280 MHz, DMSO) δ -61.42. ESI-MS $[M+Na]^+$ m/z: 547.

2.1.3 (1E,6E)-1,7-bis(4-hydroxy-3-methoxyphenyl)-4-(4-(trifluoromethyl)benzylidene)hepta-1,6-diene-3,5-dione (2c)

Yellow solid; Chemical Formula: $C_{29}H_{23}F_3O_6$; yield: 43%; mp: 185-186 ºC. IR (KBr, cm^{-1}): υ 3298, 2962, 1638, 1574, 1511, 1428, 1326, 1273, 1214, 1122. ^{1}H NMR (300 MHz, DMSO) δ 9.78 (s, 2H, OH), 8.13 (s, 1H), 7.82 (d, *J* = 8.3 Hz, 2H, Ar-H), 7.75 (d, *J* = 8.3 Hz, 2H, Ar-H), 7.71 – 7.53 (m, 2H, Ar-H), 7.48 – 7.37 (m, 2H), 7.32 (m, 2H, Ar-H), 7.11 (d, *J* = 8.2 Hz, 1H), 6.97 – 6.82 (m, 2H), 6.78 (d, *J* = 8.2 Hz, 1H), 3.88 (s, 3H, OCH_3), 3.80 (s, 3H, OCH_3). ^{13}C NMR (75 MHz, DMSO) δ 197.20, 188.50, 150.69, 150.49, 148.48, 148.45, 147.98, 145.59, 143.85, 138.40, 138.05, 130.81, 130.15(q, J = 366.75Hz), 126.56, 126.20, 126.15, 125.90, 125.55, 124.73, 124.56, 124.41(q, J = 273.75Hz), 124.33, 118.70, 116.23, 116.10, 112.80, 112.16, 56.33, 56.15. ^{19}F NMR (280 MHz, DMSO) δ -61.31. ESI-MS $[M+Na]^+$ m/z: 547.

2.1.4 (1E,6E)-4-(4-fluorobenzylidene)-1,7-bis(4-hydroxy-3-methoxyphenyl)hepta-1,6-diene-3,5-dione (2d)

Yellow solid; Chemical Formula: $C_{28}H_{23}FO_6$; yield: 73%; mp: 198-200 ºC; λ max (CH_3OH): 369; IR (KBr, cm^{-1}): υ 3293, 2957, 1633, 1594, 1516, 1458, 1277, 1229, 1161. ^{1}H NMR (300 MHz, DMSO) δ 9.81 (s, 2H, OH), 8.01 (s, 1H), 7.69 (m, 1H, Ar-H), 7.58 – 7.36 (m, 4H, Ar-H), 7.34 – 7.20 (m, 4H, Ar-H), 7.11 (m, 1H), 6.93 – 6.75 (m, 3H), 3.86 (s, 3H, OCH_3), 3.81 (s, 3H, OCH_3). ^{13}C NMR (75 MHz, DMSO) δ 196.09, 188.28, 162.85 (d, *J* = 272.7 Hz), 150.66, 150.56, 148.47,

148.43, 147.70, 146.09, 144.89, 130.80, 126.40, 125.88, 125.64 (d, *J* = 2.8 Hz), 124.81, 124.69, 124.57, 124.52, 124.48, 119.39, 119.19, 118.97, 116.19, 116.09, 112.63, 112.03, 56.28, 56.16. ^{19}F NMR (283 MHz, DMSO) δ -109.70. ESI-MS $[M+H]^+$ m/z: 475.

2.1.5 (1E,6E)-4-(2,3-difluorobenzylidene)-1,7-bis(4-hydroxy-3-methoxyphenyl)hepta-1,6-diene-3,5-dione (2e)

Yellow solid; Chemical Formula: $C_{28}H_{22}F_2O_6$; yield: 80%; mp: 197-198 ºC. IR (KBr, cm^{-1}): υ 3293, 3062, 1633, 1594, 1510, 1427, 1274, 1230. ^{1}H NMR (300 MHz, DMSO) δ 9.78 (s, 2H, OH), 8.07 (s, 1H), 7.63 (m, 4H), 7.49 – 7.36 (m, 2H), 7.36 – 7.23 (m, 3H), 7.12 (m, 1H), 7.03 – 6.75 (m, 3H), 3.88 (s, 3H, OCH_3), 3.81 (s, 3H, OCH_3). ^{13}C NMR (75 MHz, DMSO) δ 197.87, 188.43, 165.02, 161.72, 150.57, 150.30, 148.46, 148.41, 146.31 (d, *J* = 218.5 Hz), 140.61 (d, *J* = 220.5 Hz), 132.89, 132.78, 130.75, 130.71, 126.60, 125.91, 124.81, 124.44, 124.14, 118.73, 116.62, 116.34, 116.20, 116.08, 112.74, 112.12, 56.32, 56.15. ^{19}F NMR (280 MHz, DMSO) δ -138.25 (d, *J* = 21.6 Hz), -138.35 (d, *J* = 21.6 Hz). ESI-MS $[M+1]^+$ m/z: 493.

2.1.6 (1E,6E)-4-(3,4-difluorobenzylidene)-1,7-bis(4-hydroxy-3-methoxyphenyl)hepta-1,6-diene-3,5-dione (2f)

Yellow solid; Chemical Formula: $C_{28}H_{22}F_2O_6$; yield: 65%; mp: 217-219 ºC. IR (KBr, cm-1): υ 3298, 2962, 1638, 1594, 1511, 1277, 1229, 1161. ^{1}H NMR (300 MHz, DMSO) δ 9.99 (s, 2H, OH), 8.03 (s, 1H), 7.74 – 7.51 (m, 4H, Ar-H), 7.50 – 7.38 (m, 3H, Ar-H), 7.36 – 7.29 (m, 2H), 7.13 (m, 1H), 6.94 (m, 1H), 6.88 (d, *J* = 8.2Hz, 1H), 6.80 (d, *J* = 8.2 Hz, 1H), 3.88 (s, 3H), 3.82 (s, 3H). ^{13}C NMR (75 MHz, DMSO) δ 197.50, 188.34, 151.82 (d, *J* = 249.8), 150.58 , 148.46 148.17 (d, *J* = 246.5), 148.02 , 145.40, 142.63, 137.49, 131.89, 129.37, 128.67, 127.58, 126.54, 125.87, 124.64, 124.20, 119.22, 118.99, 118.81, 118.61, 116.23, 116.10, 112.79, 112.14, 56.31, 56.15. ^{19}F NMR (283 MHz, DMSO) δ -135.21 (d, *J* = 22.4 Hz), -137.48 (d, *J* = 22.5 Hz). ESI-MS $[M+H]^+$ m/z: 493.

2.1.7 (1E,6E)-4-((E/Z)-3,4-difluorobenzylidene)-1-(4-hydroxy-3-methoxyphenyl)-7-(4-hydroxyphenyl)hepta-1,6-diene-3,5-dione (3a, 3a')

Yellow solid; Chemical Formula: $C_{27}H_{20}F_2O_5$; yield: 58%; mp: 211-213 ºC. IR (KBr, cm-1): υ 3259, 1604, 1560, 1511, 1438, 1273, 1234, 1165. ^{1}H NMR (301 MHz, DMSO) δ 10.11 (s, OH, 2H), 9.86 (s, OH, 2H), 8.03 (s, H of Z/E isomers, 1H), 8.01 (s, H of Z/E isomers H, 1H), 7.73 – 7.66 (m, 1H), 7.62 (m, 2H), 7.59 – 7.48 (m, 6H), 7.47 – 7.37 (m, 5H), 7.34 – 7.28 (m, 2H), 7.13 (m, 1H), 6.98 – 6.77 (m, 7H), 3.87 (s, OMe of Z/E isomers, 3H), 3.81 (s, OMe of Z/E isomers, 2H). ^{13}C NMR (75 MHz, DMSO) δ 197.58, 197.37, 188.41, 188.12, 161.16, 160.85, 152.38, 152.21, 151.43, 151.25, 150.74, 150.44, 149.06, 148.89, 148.49, 148.44, 148.17, 148.06, 148.00, 147.59, 145.43, 144.97, 142.61, 142.58, 142.53, 142.50, 137.55, 131.96, 131.91, 131.88, 131.83, 131.60, 131.50, 127.60, 127.51, 126.56, 126.07, 125.88, 125.37, 124.62, 124.37, 124.22, 119.22, 118.99, 118.72, 118.52, 118.41, 116.44, 116.39, 116.24, 116.12, 112.76, 112.19, 56.30, 56.14. ^{19}F NMR (280 MHz, DMSO) δ -135.11, -135.12 (d, J = 22.7 Hz, F of Z/E isomers), -137.38, -137.40 (d, J = 22.7Hz, F of Z/E isomers). ESI-MS $[M+H]^+$ m/z: 463.

2.1.8 (1E,6E)-1,7-bis(4-hydroxy-3-methoxyphenyl)hepta-1,6-diene-3,5-dione (curcumin)

Chemical Formula: $C_{21}H_{20}O_6$; ^{1}H NMR (300 MHz, DMSO) δ 9.52 (s, 2H, OH), 7.43 (d, J = 15.5 Hz, 2H, C=C-H), 7.29 (s, 2H, Ar-H), 7.10 (d, J = 8.1, 2H, Ar-H), 6.81 (d, J = 8.1 Hz, 2H, Ar-H), 6.69 (d, J = 15.6 Hz, 2H, C=C-H), 6.03 (s, 2H, methylene), 3.85 (s, 6H, OCH_3).

2.2 Antiproliferative activity assay

The antiproliferative activity of the synthesized analogues was assessed by performing the MTT assay. 4T1, B16F10 and NIH 3T3 Cells were seeded at 3000 cells / well in 96-well plates after 60-70 percent confluence; cells were exposed for 72 h to synthesized analogues at different concentrations. To prepare a solution of synthesized derivatives, the prepared compound was dissolved in DMSO and subsequently diluted with RPMI 1640.

2.3 Molecular modeling

Ligands with the most antiproliferative activity and curcumin as a comparison model were selected for docking analysis. Protein-ligand interaction and ligand affinity to target were computationally investigated by Auto Dock vina. Future, a ligand with the highest affinity were determined by calculation of E-value and binding energy. 2D Synthesized Ligand Structures were drawn with ChemDraw (version 17.1). Minimization energy was performed by MOE (version 2015). After

that, resulted in 3D structure was saved as a PDB file. The key receptors were chosen based on their role in cancer, including cell division (cyclin-dependent kinase-2 (CDK2)), cell growth (mitogen-activated protein kinase (MAPK)), angiogenesis (vascular endothelial growth factor (VEGF)), cell differentiation, and migration (Akt1), cell adhesion (ABL1) and autophagy (EGFR). Gene expression, cellular growth, and survival regulate the mitogen-activated protein kinase (MAPK) pathway (16). Increased or uncontrolled cell growth may result from abnormal MAPK signaling. Cyclin-dependent kinase-2 (CDK2) belongs to the family of protein kinases. This plays a crucial function in regulating several processes in the process of eukaryotic cell division. Accumulated evidence demonstrated that an abnormal cell cycle control would result from CDK2 expression (17). Angiogenesis, or the production of new blood vessels, plays an important role in the growth and development of tumors. Thus, tumor angiogenesis inhibitors can be a promising therapeutical approach. The vascular endothelial growth factor(VEGF) is a potent and specific target for anti-cancer drugs (18). The Abelson (ABL) family nonreceptor tyrosine kinase transmits various extracellular signals to protein networks responsible for controlling proliferation, survival, migration, and invasion (19). One of the most important oncogenes typically affected in cancer is the epidermal growth factor (EGFR) receptor. It is frequently mutated or overexpressed in numerous types of human malignancies, and it is the target of several currently accepted chemotherapy drugs (20). Akt isoforms play a critical role in cancer and metastasis regulation. Surprisingly, studies have revealed that the Akt pathway is crucial for preserving the endothelial barrier and inhibiting ectopic vascular permeability, a factor in tumor metastasis. Recent findings highlight the importance of Akt in metastasis suppression (21). Crystallography structures of selected receptors including (Cyclin-Dependent Kinase 2 (1HCL), mitogen-activated protein kinase (MAPK) (2ZOQ), Insulin-Like Growth Factor-1 Receptor Kinase (3D94), Vascular Endothelial Growth Factor Receptor 2 (5EW3), ABL1 Kinase (4WA9), EGFR kinase (1XKK), Crystal structure of Akt1 (6CCY)) were obtained from the protein data bank. Protein structures and ligands were converted into a PDBQT file by Auto Dock tools (Version1.5.6). To measure the number of formed hydrogen bonds and binding energy, synthesized ligands were docked against targets by Auto Dock vina.

2.4 Molecular Dynamics Simulation

The docking analysis selected a protein with the highest affinity and lowest binding energy with ligands for molecular dynamics simulation. The top pose of ligand protein from docking results

was selected and converted to a pdb file by MOE software. The molecular dynamics simulation on the ligand-protein and empty protein was performed by GROMACS v2018 with force field CHARMM36. Ligand-protein and empty protein were immersed in the middle of a dodecahedron water box with the TIP3P model and neutralized by adding Na^+ and Cl^- ions. The system's energy was minimized, and the solvent and ions around of systems were balanced in two phases (NVT ensemble and NPT ensemble). Finally, the molecular dynamic simulation was performed on the ligand-protein complex and protein empty.

2.5 Statistical analysis

Statistical analyses were performed using GraphPad Prism 8 (GraphPad Software, Inc., San Diego, CA). Between-group comparisons were made using one-way ANOVA with Tukey-Kramer test for posthoc multiple comparisons. A two-sided p-value of <0.05 was considered significant.

3 Results and discussion

3.1 Synthesis and characterization of curcumin analogues

A series of fluorinated curcumin and fluorinated DMC were synthesized by Knoevenagel condensation between curcumin or DMC and fluorinated benzaldehydes.

Figure legends

Figure *1* provides a graphical summary of the synthesis process. At room temperature, the condensation of fluorinated benzaldehyde (**1a-1f**) in methanol with curcumin or DMC in the presence of the catalyst, piperidine, was carried to generate the fluorinated compounds (**2a-2f** and **3a**). The structure of fluorinated compounds was confirmed by ^{1}HNMR, ^{13}CNMR, ^{19}FNMR and FTIR. Compound **2a** (Figure 2) is chosen as a descriptive compound to confirm the structures of the synthesized compounds. The FT-IR spectrum of compound **2a** shows absorption frequencies around 3308 $cm^{-1,}$ and the absorption bands observed around 2962, 1632 cm^{-1}. In the ^{1}HNMR spectrum of **2a**, two singlet width signals were appeared in around 9.8 ppm, and a characteristic singlet peak with integral one proton was observed in around 8.05 ppm. The aromatic protons were observed in the region of 7.7–6.8 ppm. Two strong singlet signals appeared around 3.8 ppm. In the ^{13}C NMR spectrum of **2a**, two ^{13}C resonances appeared at 196.65, 188.39 ppm and two characteristic resonance observed at 56.29, 56.16 ppm. Mass spectrum of compound **2a** showed a molecular ion peak at m/z: 475$[M+H]^{+}$. More results are presented in the supplementary materials.

Figure 2

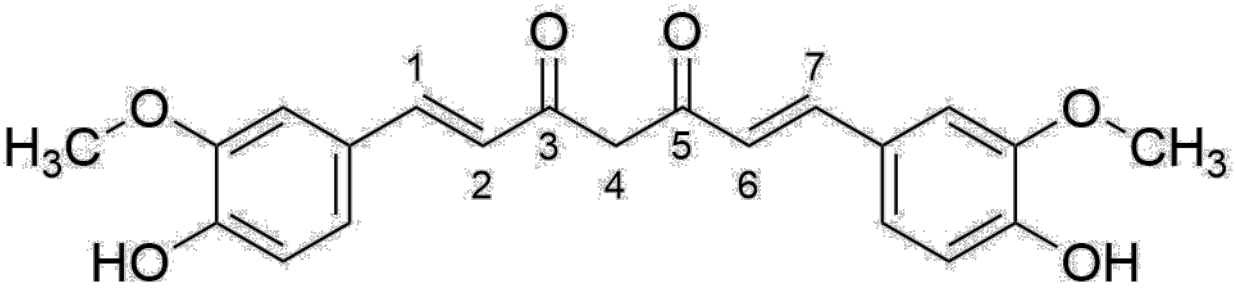

Curcumin

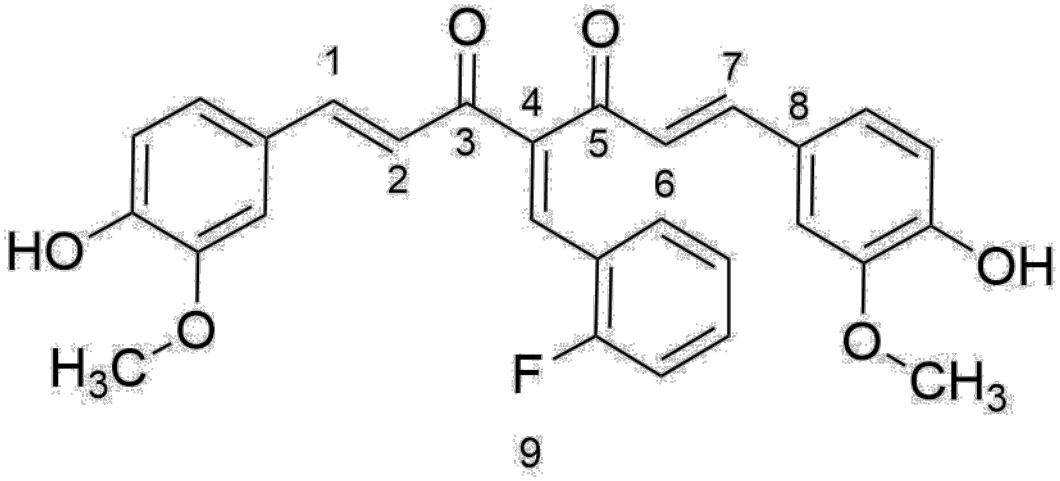

2a

3.2 Antiproliferative activity analysis

The antiproliferative activity of fluorinated compounds was assessed by MTT assays in murine metastatic melanoma cell lines B16F10, mouse breast cancer 4T1 cell line, and human NIH 3T3(normal cell line) cell line. Compared to the NIH cell line, synthesized compounds showed a stronger ability to suppress melanoma and breast cancer cells. Results of antiproliferative activity are summarized in **Error! Reference source not found.** suggesting that all synthesized compounds significantly inhibited the proliferation of cancer cell lines in the micromolar range (0.5–5.6μM) compared with curcumin. Compounds **2f** and **3a** showed the most inhibition of cancer cell proliferation. Compounds **2b** and **2c** containing trifluoromethyl moiety showed lower potency than other fluorinated compounds.

Table 1

	B16F10	4T1	NIH 3T3
		IC50/μM	
Curcumin	15.5	30.0	29.1
2a	0.90	1.75	22.7
2b	2.20	3.20	15.3
2c	3.39	5.67	17.7
2d	0.95	0.94	20.6
2e	0.72	2.76	31.5
2f	0.59	0.79	24.4
3a	0.89	0.96	29.3

3.3 Molecular docking study

According to the results of the MTT assay, compounds **2f** and **3a** were selected as the most potent inhibitors for molecular docking analysis. To calculate the E-value and affinity of ligand-protein complexes, docking analysis was performed by Auto Dock vina. The results as illustrated in Table 2 showed affinity rank-order of compound **2f** against proteins was as EGRF > ILGF-1 > CDPK-2 > MAK-ERK-1 > VEGF > Serine/threonine-protein kinase AKT > Tyrosine-protein kinase ABL1 and **3a** affinity rank-order against proteins was found as EGRF > Tyrosine-protein kinase ABL1 and Serine/threonine-protein kinase AKT > ILGF-1 > MAK-ERK-1 > CDPK-2> VEGF. On the other hand, curcumin affinity rank-order against proteins was found as Tyrosine-protein kinase ABL1 > VEGF > CDPK-2 > Serine/threonine-protein kinase AKT > EGRF > by cMAK-ERK-1 > ILGF-1. The results indicated (Table 2) that compounds **2f** and **3a** exhibited the highest affinity (-10.0 and -9.80 kcal/mol, respectively) with epidermal growth factor receptor (EGFR). Curcumin, as the parent compound, showed weak affinity (-7.8 kcal/mol) with EGFR. Compound **2f** and **3a** bond to EGFR by formation 3 and 2 hydrogen bonds, respectively. Lapatinib is a standard inhibitor of EGFR with E-value -11.2 Kcal/mol bond to target by formation 4 hydrogen bonds.

3.4 Molecular dynamic simulation

Molecular dynamic simulations were used to compare the obtained structural differences when proteins were bound to different ligands. According to docking analysis, the EGFR (PDB: 1KXX) was selected to assess the time-dependent behaviour of EGFR against compounds **2a**, **3f** and

curcumin. The conformational stability of EGFR in ligand-protein complex and EFGR alone (apo-form) was evaluated with the calculation of Root-Mean-Square Derivations (RMSD) and radius of gyration (Rg) in 100 ns simulations. The RMSD plot (Figure 3) showed an increase in the RMSD value of the curcumin-EGFR complex during the simulation. The RMSD value increased from 0.2 nm to 0.4 nm in the initial 19 ns of simulation after remained constant, with an average of 0.35 nm to 44 ns. Again, the RMSD value increased from about 0.35 nm to 0.6 nm until 46 ns. The RMSD value then fluctuated and decreased to approximately 0.4 nm until the simulation was completed. The obtained results showed that the complex 2f-EGFR or 3a-EGFR and apo-form tolerate low variations during molecular docking (MD). The radius of gyration (Rg) was determined to evaluate EGFR stability in complex with **2f**, **3a** and curcumin. Rg value of curcumin-EGFR was increased more than Rg of **2a** or **3a**-EGFR and apo-form (Figure 4). Rg value of curcumin-EGFR increased during the initial 30 ns of simulation from around 2 nm to 2.05 nm after it decreased and remained stable until 44ns for 14 ns. Then Rg of curcumin-EGFR increased to about 2.06 nm until 70 ns. Then the Rg value fluctuated and reduced to about 2.0 nm until simulation was completed. The hydrogen bonds play an essential role in protein folding, secondary protein structure, alpha helices and protein function. The results showed that (Figure 5 and 6) the methoxy group of **2f** interact with ASP-91 moiety via hydrogen. The carbonyl group of **2f** and **3a** formed a hydrogen bond with LYS-40. The hydroxyl and methoxy groups of curcumin interact with ASP-91 through the formation of a hydrogen bond.

Figure 3

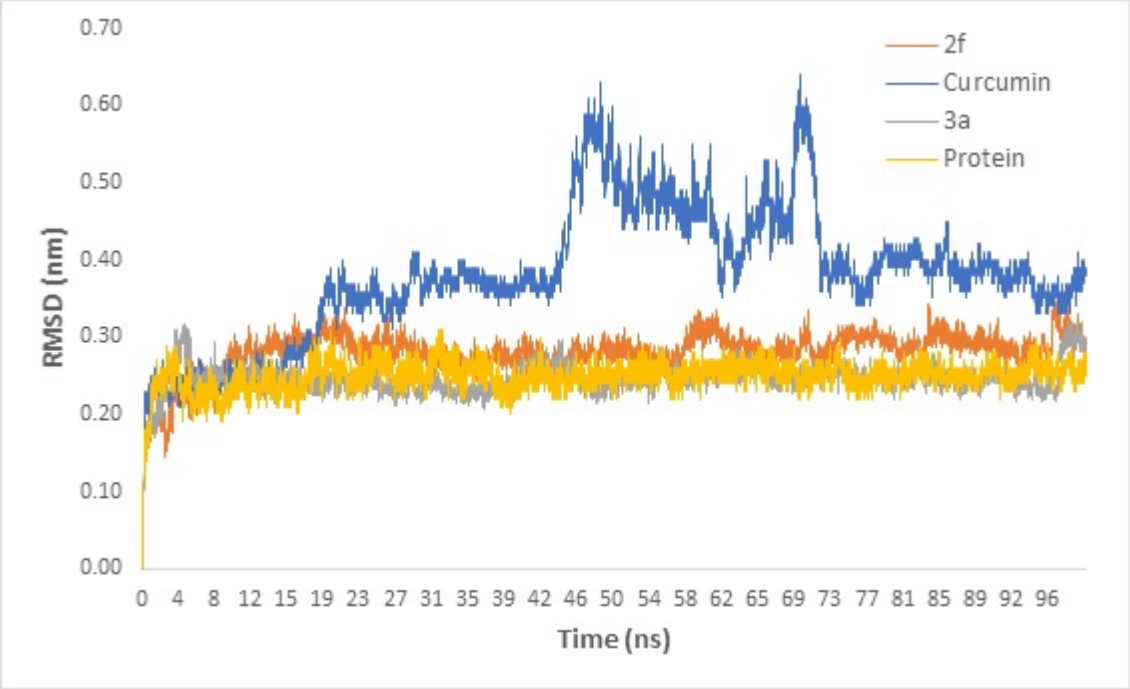

Figure 4

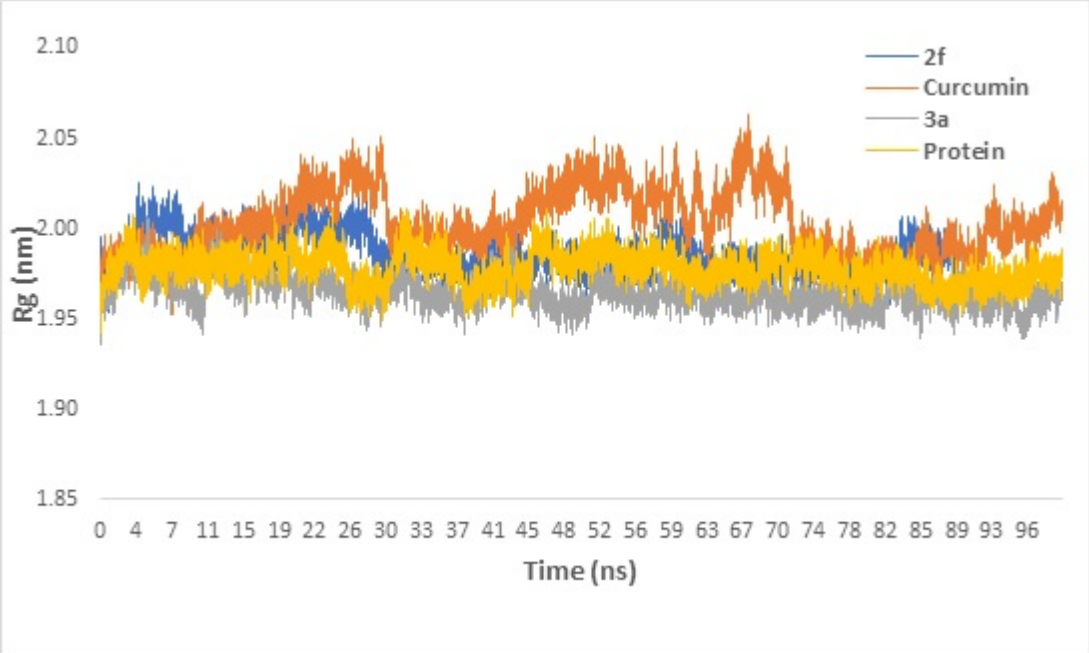

Figure 5

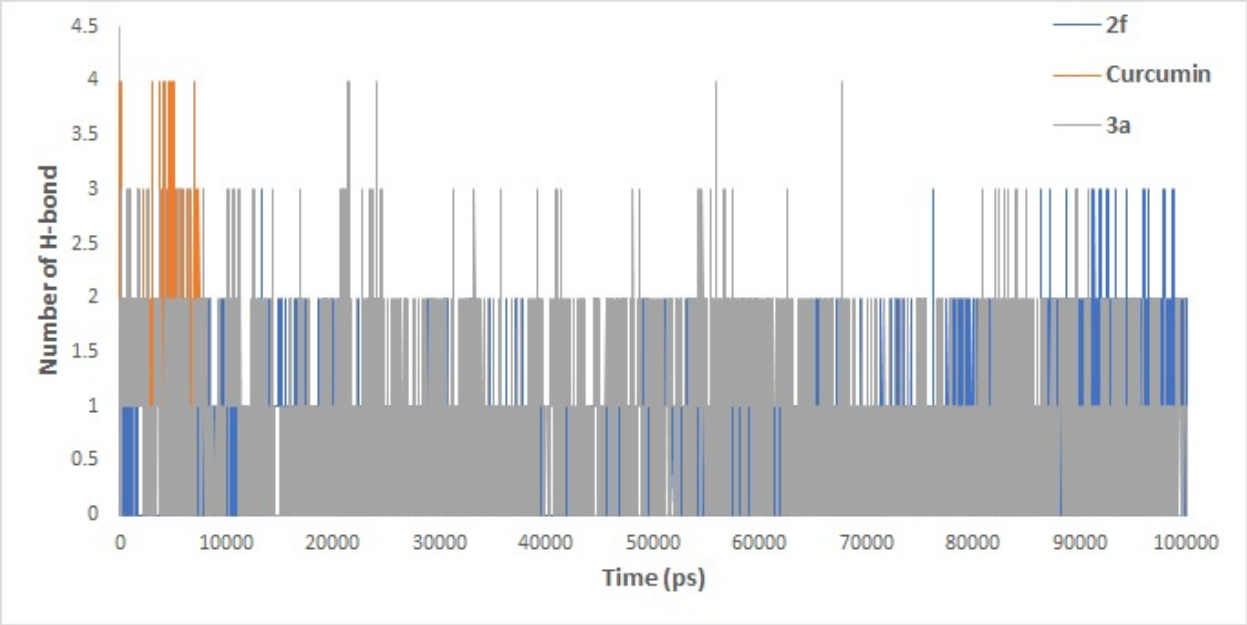
2f
Curcumin
3a
Number of H-bond
Time (ps)
0
0.5
1
1.5
2
2.5
3
3.5
4
4.5
0
10000
20000
30000
40000
50000
60000
70000
80000
90000
100000

2f

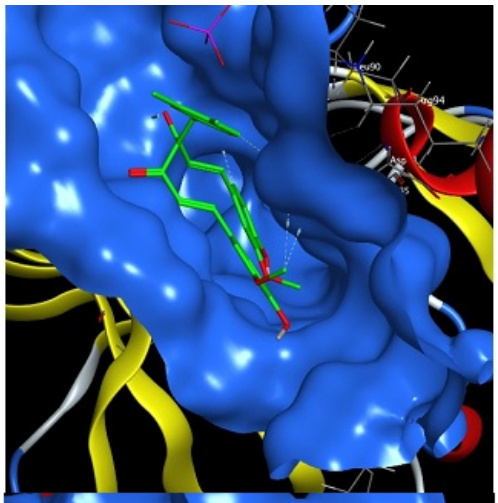

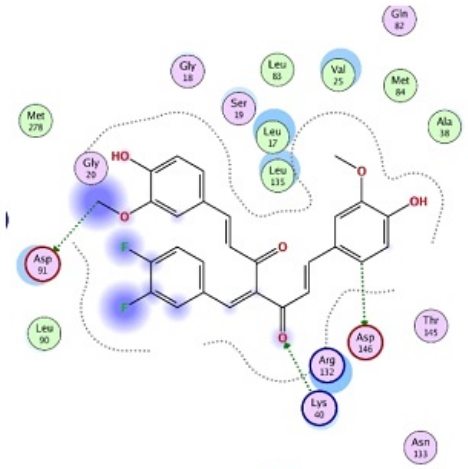

3a

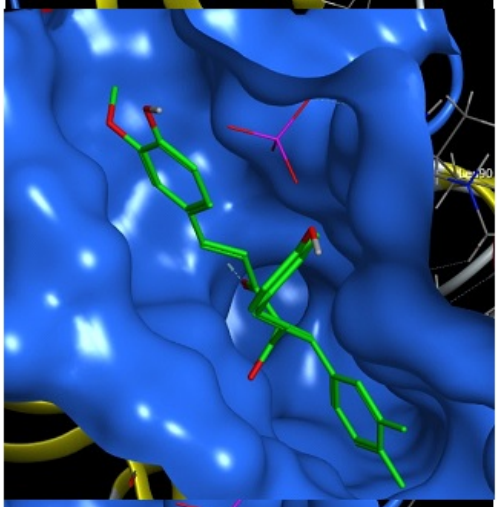

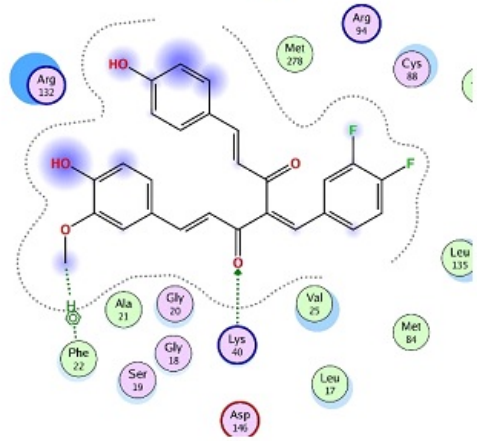

Curcumin

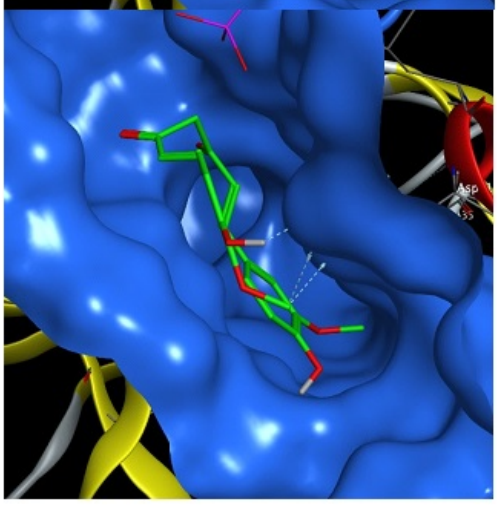

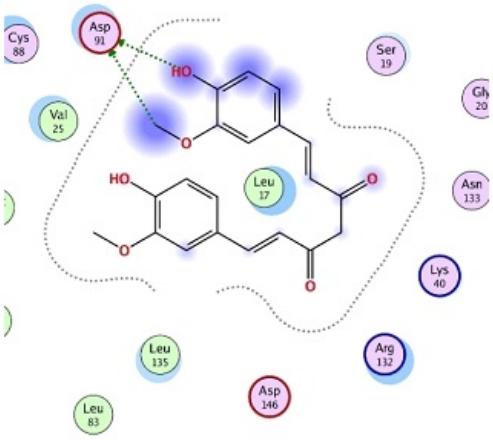

4 Discussion

Curcumin, a symmetrical molecule abundant in turmeric, has been shown in clinical and preclinical investigations to have various health-boosting properties, including antioxidant, antibacterial, anti-inflammatory, and anticancer characteristics. However, curcumin has a low oral bioavailability, which has been suggested to be a potential factor minimizing its pharmacological efficacy (2). Consequently, numerous drug delivery systems have been designed and tested to improve the pharmacokinetic profile of this phytochemical, including liposomes, micelles, phospholipids complexes and nanoparticles. To date, efforts to prevent the rapid metabolism of curcumin have had minimal effectiveness. This has prompted researchers to develop innovative synthetic curcumin analogues in an attempt to solve the challenges of low bioavailability and rapid metabolism, as well as to increase potency while minimizing toxicity. Recently, many studies reported that 4-arylidene curcumin derivatives demonstrate greater anti-cancer activity than curcumin against some cancers, making them potential candidates for further research and development (22). A related approach showed that the fluorinated 4-arylidene curcumin was metabolically stable, and its blood circulation time was improved. In this study, a series of fluorinated curcumin and fluorinated DMC analogues were synthesized by Knoevenagel condensation between curcumin or DMC and fluorinated benzaldehydes. To confirm condensation, a comparison evaluation was performed between spectroscopic results of synthesized compound and curcumin. ^{1}HNMR spectrum of the synthesized compound showed a singlet peak which appeared around 8 ppm, while this signal was not observed in the spectrum of curcumin. In addition, a singlet peak appeared at 6.03 ppm corresponded to H-4 of curcumin, while this signal did not appear in the ^{1}HNMR spectrum of the synthesized compound. Signal corresponded to methoxy groups of curcumin appeared at 3.85ppm as a singlet signal with 6 protons integral. Due to condensation, methoxy groups of the synthesized compound showed two signals around 3.8 ppm. Due to the enol form of curcumin, the FT-IR spectrum of curcumin exhibited the carbonyl stretching frequency at 1628 $cm^{-1,}$ while in the FT-IR spectrum of synthesized compounds (**2a**-**2f** and **3a**), the carbonyl bond shifted to higher frequencies and appeared around 1638–1633 cm^{-1}. To confirm the structures of the synthesized compounds, compound **2a** is chosen as a representative compound. The absorption frequencies around 3308 cm^{-1} observed in the FT-IR spectrum of compound **2a** are due to aromatic CH stretching vibration. The absorption bands observed around 2962 correspond to the aliphatic CH stretching vibrations.

The appeared bond around 1632 cm^{-1} is due to carbonyl stretching vibration. In the ^{1}HNMR spectrum of **2a**, two singlet width signals corresponded to hydroxyl groups appeared in around 9.8, ppm and a characteristic singlet peak with integral one proton was observed in around 8.05 ppm due to H-9 (Figure 2). Two strong singlet signals appeared around 3.8 ppm due to the presence of proton on methoxy groups. In the ^{13}C NMR spectrum of **2a**, two ^{13}C resonance of carbonyls groups appeared at 196.65, 188.39 ppm and two characteristic resonance observed at 56.29, 56.16 ppm due to carbon presence at methoxy groups. The mass spectrum of compound **2a** showed a molecular ion peak at m/z: 475$[M+H]^{+}$ by adding a proton consistent with the proposed molecular mass. Demethoxycurcumin is an asymmetric molecule and produces two Z/E isomers as a result of Knoevenagel condensation. Two signal series were observed in the ^{1}H NMR spectrum of **3a** due to the Z/E isomers molecule. The Z/E isomers ratio was calculated from the area under the curve of the proton on C=C-H groups. The results showed a 60:40 ratio between Z/E isomers. Recent studies have shown that the proliferation of human breast cancer and melanoma cells has been significantly suppressed by curcumin in a dose/time-dependent manner (23, 24). In this study, we assessed the antiproliferative activity of synthesized on breast and melanoma cell lines. the synthesized compound (**2a**-**2f** and **3a**) demonstrated higher activity against 4T1 and B16F10 cancer cells than curcumin. Also, it was discovered that the proposed derivatives attenuated the proliferation of two cancer cells better than the 3T3/NIH cells. The compounds containing fluorinated benzyl groups were significantly more toxic against cancer cells. The results showed that the substitution of 4-arylidene groups has improved activity against cancer cell growth. This suggestion is backed up by the evidence in (22) which, supports this idea. Docking was utilized to evaluate ligands affinity to their corresponding protein targets. Autodock Vina software (25) was used to dock compounds (**2f** and **3a)** with the highest antiproliferative activity. In this analysis, some parameters such as E-value and hydrogen bonds were evaluated, showing that the compounds **2f** and **3a** showed the highest affinity to EGFR. Also, It has been shown that curcumin prevents the development of cancer cells via inhibition of EGFR, HER2, MAPK, phosphorylase kinase, pp60c-src tyrosine kinase, protein kinase C and protein kinase A (26, 27). One investigation reported that curcumin selectively inhibits cancer cells through the suppression of EGFR(28). Based on the docking analysis, EGFR was the most potential candidate target that fluorinated curcumin derivatives can act as its inhibitor. MD simulations were conducted to evaluate the stability of binding poses obtained from molecular docking of EGFR in

complex with fluorinated derivatives (**2f** and **3a)** and curcumin. The average distance between the atoms of overlaid proteins is evaluated by the root-mean-square deviation (RMSD) of atomic positions. By calculating the root mean square deviation (RMSD) from the original structure in MD simulations, the structural stability of EGFR-ligand complexes in TIP3P solvents and the neutralized system has been evaluated. At the end of MD simulations, RMSD of the EGFR-ligand complex (**2f** and **3a**) seemed to fit perfectly in the EGFR binding pocket and proved to form stable complexes. While the curcumin RMSD shows a fluctuation, it appears due to instability in the EGFR's structure. Consequently, **3a** improved the conformational stability of EGFR more than curcumin. The root-mean-square space among all atoms in a molecule and the midpoint, calculated by the macromolecule structural compactness, determines the radius of gyration (Rg)(29). Rg indicates the compactness of the structure, in particular in the analysis of protein. For some 30 ns of simulation, the Rg value of EGFR-curcumin was raised. While the rg of EGFR-**2f** and **3a** were observed to be consistent. This implied that the EGFR could maintain its innate conformation during MD and maintain contact with fluorinated derivatives from 0 to 30 ns. In comparison, the EGFR structure showed ability with curcumin in 30 ns MD. Hydrogen bonds play an important role in the ligand-protein complex. The results demonstrated that **2f** and **3a** formed three to four protein hydrogen bonds and enhanced ligand affinity to EGFR. Surprisingly, the data indicate a hydrogen bond formed between the H-N atom of LYS 41 and the O-atom at the carbonyl group of **2f** and **3a**. Curcumin and **3a**, on the other hand, have fascinating hydrogen bond pairs with ASP91.

5 Conclusion

In summary, a novel series of fluorinated analogues of curcumin and DMC were synthesized, and the resulted compounds strongly inhibited cancer cell growth. Two compounds (**2f** and **3a)** were validated by showing significant binding interactions with the receptor. MD analysis showed that compounds **2f** and **3a** improved the stability of EGFR and enhanced affinity via the formation of hydrogen bonds with EGFR. These new curcuminoids with potent anti-tumor activities could present potential opportunities for therapeutic progress against cancer. Further validation of the anti-tumor activities of these identified compounds in relevant cell-based and animal models is warranted.

Consent for Publication

Not applicable.

Conflict of Interest

Declared none.

Acknowledgements

Declared none.

References

1. Hatamipour M, Johnston TP, Sahebkar AJCpd. One molecule, many targets and numerous effects: the pleiotropy of curcumin lies in its chemical structure. 2018;24(19):2129-36.
2. Anand P, Kunnumakkara AB, Newman RA, Aggarwal BBJMp. Bioavailability of curcumin: problems and promises. 2007;4(6):807-18.
3. Sardjiman S, Reksohadiprodjo M, Hakim L, Van der Goot H, Timmerman HJEJoMC. 1, 5-Diphenyl-1, 4-pentadiene-3-ones and cyclic analogues as antioxidative agents. Synthesis and structure-activity relationship. 1997;32(7-8):625-30.
4. Tomren M, Masson M, Loftsson T, Tønnesen HHJIjop. Studies on curcumin and curcuminoids: XXXI. Symmetric and asymmetric curcuminoids: stability, activity and complexation with cyclodextrin. 2007;338(1-2):27-34.
5. Fang L, Gou S, Liu X, Cao F, Cheng LJB, letters mc. Design, synthesis and anti-Alzheimer properties of dimethylaminomethyl-substituted curcumin derivatives. 2014;24(1):40-3.
6. Fang X, Fang L, Gou S, Cheng LJB, letters mc. Design and synthesis of dimethylaminomethyl-substituted curcumin derivatives/analogues: Potent antitumor and antioxidant activity, improved stability and aqueous solubility compared with curcumin. 2013;23(5):1297-301.
7. Qiu X, Du Y, Lou B, Zuo Y, Shao W, Huo Y, et al. Synthesis and identification of new 4-arylidene curcumin analogues as potential anticancer agents targeting nuclear factor-κB signaling pathway. 2010;53(23):8260-73.
8. Smart BE. Introduction: fluorine chemistry. ACS Publications; 1996.
9. Padhye S, Yang H, Jamadar A, Cui QC, Chavan D, Dominiak K, et al. New difluoro Knoevenagel condensates of curcumin, their Schiff bases and copper complexes as proteasome inhibitors and apoptosis inducers in cancer cells. 2009;26(8):1874-80.
10. Anand P, Thomas SG, Kunnumakkara AB, Sundaram C, Harikumar KB, Sung B, et al. Biological activities of curcumin and its analogues (Congeners) made by man and Mother Nature. 2008;76(11):1590-611.
11. Katsidoni V, Alexiou P, Fotiadou M, Pelecanou M, Sagnou M, Panagis GJP. Curcumin, demethoxycurcumin and bisdemethoxycurcumin differentially inhibit morphine's rewarding effect in rats. 2014;231(23):4467-78.
12. Yodkeeree S, Chaiwangyen W, Garbisa S, Limtrakul PJTJonb. Curcumin, demethoxycurcumin and bisdemethoxycurcumin differentially inhibit cancer cell invasion through the down-regulation of MMPs and uPA. 2009;20(2):87-95.
13. Liu Y-L, Yang H-P, Gong L, Tang C-L, Wang H-JJMmr. Hypomethylation effects of curcumin, demethoxycurcumin and bisdemethoxycurcumin on WIF-1 promoter in non-small cell lung cancer cell lines. 2011;4(4):675-9.

14. Shieh J-M, Chen Y-C, Lin Y-C, Lin J-N, Chen W-C, Chen Y-Y, et al. Demethoxycurcumin inhibits energy metabolic and oncogenic signaling pathways through AMPK activation in triple-negative breast cancer cells. 2013;61(26):6366-75.
15. Lin H-Y, Lin J-N, Ma J-W, Yang N-S, Ho C-T, Kuo S-C, et al. Demethoxycurcumin induces autophagic and apoptotic responses on breast cancer cells in photodynamic therapy. 2015;12:439-49.
16. Knight T, Irving JAE. Ras/Raf/MEK/ERK pathway activation in childhood acute lymphoblastic leukemia and its therapeutic targeting. Frontiers in oncology. 2014;4:160.
17. Chohan TA, Qian H, Pan Y, Chen J-Z. Cyclin-dependent kinase-2 as a target for cancer therapy: progress in the development of CDK2 inhibitors as anti-cancer agents. Current medicinal chemistry. 2015;22(2):237-63.
18. Verheul HM, Pinedo HM. The role of vascular endothelial growth factor (VEGF) in tumor angiogenesis and early clinical development of VEGFReceptor kinase inhibitors. Clinical Breast Cancer. 2000;1:S80-S4.
19. Greuber EK, Smith-Pearson P, Wang J, Pendergast AM. Role of ABL family kinases in cancer: from leukaemia to solid tumours. Nature Reviews Cancer. 2013;13(8):559-71.
20. Sigismund S, Avanzato D, Lanzetti L. Emerging functions of the EGFR in cancer. Molecular oncology. 2018;12(1):3-20.
21. Alwhaibi A, Verma A, Adil MS, Somanath PR. The unconventional role of Akt1 in the advanced cancers and in diabetes-promoted carcinogenesis. Pharmacological research. 2019;145:104270.
22. Vyas A, Dandawate P, Padhye S, Ahmad A, Sarkar FJCpd. Perspectives on new synthetic curcumin analogs and their potential anticancer properties. 2013;19(11):2047-69.
23. Pisano M, Dettori MA, Fabbri D, Delogu G, Palmieri G, Rozzo C. Anticancer Activity of Two Novel Hydroxylated Biphenyl Compounds toward Malignant Melanoma Cells. International Journal of Molecular Sciences. 2021;22(11):5636.
24. Koohpar ZK, Entezari M, Movafagh A, Hashemi M. Anticancer activity of curcumin on human breast adenocarcinoma: Role of Mcl-1 gene. Iranian journal of cancer prevention. 2015;8(3).
25. Dallakyan S, Olson AJ. Small-molecule library screening by docking with PyRx. Chemical biology: Springer; 2015. p. 243-50.
26. Dorai T, Gehani N, Katz AJMu. Therapeutic potential of curcumin in human prostate cancer. II. Curcumin inhibits tyrosine kinase activity of epidermal growth factor receptor and depletes the protein. 2000;4(1):1-6.
27. Yim-Im W, Sawatdichaikul O, Semsri S, Horata N, Mokmak W, Tongsima S, et al. Computational analyses of curcuminoid analogs against kinase domain of HER2. 2014;15(1):261.
28. Xu Y-Y, Cao Y, Ma H, Li H-Q, Ao G-ZJB, chemistry m. Design, synthesis and molecular docking of α, β-unsaturated cyclohexanone analogous of curcumin as potent EGFR inhibitors with antiproliferative activity. 2013;21(2):388-94.
29. Lobanov MY, Bogatyreva N, Galzitskaya O. Radius of gyration as an indicator of protein structure compactness. Molecular Biology. 2008;42(4):623-8.

Figure legends

Figure 1. Synthesis of fluorinated curcumins and fluorinated DMC; Reagents and conditions: a) MeOH, piperidine, rt, 48h.

Figure 2. Molecular structure of **2a** and curcumin

Figure 3. RMSD plot of EGFR with **2f**, **3a**, curcumin, and EGFR alone.

Figure 4. Rg of EGFR with ligand (**2f**, **3a**, curcumin) and without ligand.

Figure 5. Number of generated hydrogen bonds between EGFR and ligands (**2f**, **3a**, and curcumin).

Figure 6. A diagram of interactions between EGFR and ligands (compounds **2f**, **3a** and curcumin) in the active site following molecular dynamic simulation (100ns).

Table 1. Antiproliferative activity (IC50 in μM) of compounds **2a**, **2b**, **2c**, **2d**, **2e**, **2f** and **3a**) in metastatic melanoma cancer (B16F10), breast cancer(4T1) and human NIH 3T3 cell lines.

	B16F10	4T1	NIH 3T3	P value	
	IC50/μM			**NIH vs. 4T1**	**NIH vs. B16F10**
Curcumin	15.5	30.0	29.1	<0.0001	<0.0001
2a	0.90	1.75	22.7	<0.0001	<0.0001
2b	2.20	3.20	15.3	<0.0001	<0.0001
2c	3.39	5.67	17.7	<0.0001	<0.0001
2d	0.95	0.94	20.6	<0.0001	<0.0001
2e	0.72	2.76	31.5	<0.0001	<0.0001
2f	0.59	0.79	24.4	<0.0001	<0.0001
3a	0.89	0.96	29.3	<0.0001	<0.0001

Table 2. E-value (Kcal/mol) and post-docking analysis of best pose of **2f**, **3a**, curcumin, and standard drugs with cyclin-dependent protein kinase-2 (CDPK-2), mitogen-activated kinase (MAK-ERK-1), insulin-like growth factor-1 (ILGF-1), vascular endothelial growth factor (VEGF), Tyrosine-protein kinase ABL1, Epidermal Growth Factor Receptor (EGFR) and Serine/threonine-protein kinase

Target	PDB-ID's	Curcumin			2f			3a			Standard Drugs			
		E value Kcal/mol	No of H-Bonds	Binding residues	E value Kcal/mol	No of H-Bonds	Binding residues	Kcal/mol	No of H-Bonds	Binding residues	Standard	E value Kcal/mol	No of H-Bonds	Binding residues
CDPK-2	1HCL	-7.9	1	ASP 145	-9.6	3	LYS-89 GLN-131 THR-14	-9.2	3	LYS-89 LYS-129 THR-14	Sunitinib	-8.6	4	THR-14 LYS -129 GLN -131 LYS -33
MAK-ERK-1	2ZOQ	-7.0	2	SER-219 ASP-196	-9.49	3	THR-223 SER-225 ASP-196	-9.41	2	ASN-316 SER-225	Sunitinib	-9.0	5	ASN-316 THR-223 SER-225, 219 ASP-196
ILGF-1	3D94	-6.2	0	-	-9.83	1	ARG-973 MET-1052	-9.63	2	ARG-973 MET-1052	PQIP	-15.96	2	MET-1052 LYS-1003
VEGF	5EW3	-8.4	1	ASN-923	-9.35	2	CYS-919 ASP-1046	-8.97	1	ALA-881	AAL993	-4.7	1	GLN-1137
Tyrosine-protein kinase ABL1	4WA9	-8.9	1	MET-318	-8.89	1	GLU 255	-9.68	1	TYR 253	**Axitinib**	-11.07	2	MET-318 ASP-381
EGFR	1XKK	-7.80	1	ASP-91	-10.0	3	ASP-146 ASP-91 LYS-40	-9.80	2	LYS-40 PHE-22	**lapatinib**	-11.2	4	ASP-91 GLN-82 LEU-79 LEU-17

Serine/threonine-protein kinase	6CCY	-7.5	2	THR-211 ASP-292	-9.21	1	GLU-234	-9.68	0	-	**inhibitor**	-10.23	1	ALA-230

Table 3. E-value (Kcal/mol) and post-docking analysis of best pose of **2f**, **3a**, curcumin, and standard drugs with cyclin-dependent protein kinase-2 (CDPK-2), mitogen-activated kinase (MAK-ERK-1), insulin-like growth factor-1 (ILGF-1), vascular endothelial growth factor (VEGF), Tyrosine-protein kinase ABL1, Epidermal Growth Factor Receptor (EGFR) and Serine/threonine-protein kinase